Steam reforming of clean biogas over Rh and Ru open-cell metallic foam structured catalysts

Steam reforming of clean biogas over Rh and Ru open-cell metallic foam structured catalysts

Pilar Tarifa,[1,2,§] Nicola Schiaroli,[1,§] Phuoc Hoang Ho,[1,†] Fernando Cañaza,[2] Francesca Ospitali,[1] Giancosimo Sanghez de Luna,[1] Carlo Lucarelli,[3] Giuseppe Fornasari,[1] Angelo Vaccari,[1] Antonio Monzon,[2] Patricia Benito[1,*]

[1]Dipartimento di Chimica Industriale "Toso Montanari", Viale Risorgimento 4, 40136, Bologna, Italy

[2]Instituto de Nanociencia y Materiales de Aragón-INMA, (CSIC-University of Zaragoza), Zaragoza (Spain)

[3]Dipartimento di Scienza e Alta tecnologia, via Valleggio 9, 22100, Como, Italy

§ P. Tarifa and N. Schiaroli contributed equally

[†]Present address: Chemical Engineering, Competence Centre for Catalysis, Chalmers University of Technology, SE-412 96 Gothenburg, Sweden

Abstract

The valorisation of clean biogas (CH_4/CO_2 = 60/40 v/v) by steam reforming over metal open-cell foam-based structured catalysts was investigated. NiCrAl foams were coated by RuMgAl or RhMgAl hydrotalcite-type compounds through electrodeposition to obtain, after calcination, a thin and stable catalytic film of oxides. The active sites for the reforming reactions are highly dispersed Rh or Ru nanoparticles stabilized by a strong metal support interaction, large Ni particles segregated from the support during reduction and reaction, and Rh/Ni bimetallic particles formed by the interaction of the two formers. Rh-based catalysts show superior activity and stability with the time on stream than Ru catalyst, and a low carbon deposition, which is mainly ascribable to the presence of larger Ni particles. In comparison to a pelletized catalyst, the structured catalysts were allowed to operate at high space velocities and low Steam to CH_4 ratio, increasing the biogas valorisation and thus the productivity.

Keywords: Clean Biogas, reforming, open-cell foam, Rh, Ni

1. Introduction

Clean biogas produced by anaerobic digestion of biomass and/or organic wastes, pre-treated to remove sulfur and other undesirable components as ammonia or siloxanes, can be valorized in delocalized small plants through reforming processes, converting CH_4 and CO_2 into syngas (CO + H_2). The direct conversion through Biogas Dry Reforming (BDR) has the potential to fully exploit the biogas content and to mitigate the environmental challenges associated with green house gas (GHG) emission. However, this process has many limitations related to its remarkable endothermicity (ΔH^0_{298K} =247 kJ/mol), the high carbon formation rate and the catalyst deactivation observed at the harsh reaction conditions needed [1]. Different operational configurations have been proposed to deal with heat issues, carbon formation and exit composition of the syngas [2]. The addition of steam reduces carbon formation and leads to a syngas composition with exploitable H_2/CO values close to 2 [3]. In the case of Steam Reforming of Biogas (BSR), the simultaneous reactions of CH_4 with CO_2 and H_2O are highly endothermic, and the use of a high steam/CH_4 (S/CH_4) ratio increases the H_2 selectivity, but significantly suppresses the CO_2 conversion [4-7].

Noble and transition metal-based catalysts have been extensively studied to promote the reforming reactions. Due to their lower price, Ni-based catalysts are widely used in the combined steam reforming (SR) and dry reforming (DR) of CH_4 [8-10], albeit their tendency to re-oxidation [11], sintering, and poor resistance against carbon formation cause major operational drawbacks, especially at low S/CH_4 values [4,12]. Rh [13-14] and Ru [15-17] overcome the Ni drawbacks since they are very active in reforming processes and less prone to carbon formation, however, their loading in the catalytic formulation should be minimized to reduce the catalyst cost. Nickel-noble metal bimetallic catalysts represent a good compromise between associated costs and catalytic activity. Ru-Ni catalysts show a lower tendency to coke deposition in the combined steam and dry reforming [18] owed to the Ru-Ni interaction, which improved carbon gasification as demonstrated by other studies on DR reaction [19,20]. The co-presence of Rh and Ni, modifies the electronic

properties of the latter, promoting its reducibility and dispersion, avoiding the sintering of the metallic particles [21-23].

The properties of the support, such as thermal stability [24], oxygen storage capacity [13,25-27] and basicity [8,28,29] as well as the distribution and interaction of the active species with the support [8,30], are of paramount importance since they control the sintering phenomena and the formation of carbonaceous species on the surface of the catalyst, as well as the activation routes of H_2O and CO_2. For instance, the oxygen storage capacity of CeO_2 [13,26] and the basicity of Ca, Mg and La enhances the resistance to the formation of carbonaceous deposits [8,31]. While the confinement or embedment of Ni on the support forms well-dispersed Ni particles that are resistant against sintering [32,33]. Bulk hydrotalcite-type (HT) derived catalysts (e.g. RhNiMgAl, NiMgCeAl) show a strong metal-support interaction, well dispersed metal particles and a surface basicity that enhances CO_2 conversion and assure high catalytic activity and stability [32,34,35].

The choice of the catalyst formulation is a key factor in the steam reforming of the biogas, but also on the heat transfer issues. The combination of both highly endothermic SR and DR reactions in the reactor provokes a decrease in the temperature, and in turn, may affect the activity. Structured catalysts, especially those made by metallic supports, enhance mass and heat transfer rates and decrease pressure drop, thus being an optimum choice to decrease temperature gradients working at high GHSV under transient conditions [36].

Ni and/or noble metal-based catalysts deposited on honeycomb monoliths or open-cell foams have been proposed for the BSR as well as for the single DR and SR of CH_4 reactions. A Ni-containing catalyst, promoted with small amounts of Ru, coated on cordierite monoliths shows an enhanced activity in the dry reforming of CH_4 in comparison to a packed bed reactor; however, the enhancement is related to the larger contact time over the monolith rather than to the effect of the structured support itself [19]. Replacing the cordierite honeycomb monoliths (500 cells per square inch, cpsi) with Al_2O_3 (30 pores per inch, ppi) open-cell foams improves the performance in the

steam reforming of biogas with Ni/CeO_2 and Ni-Rh/CeO_2 catalysts [37]. The tortuous geometry of foams favours the gas-solid interaction and therefore the heat and mass transfer, while still keeping an acceptable pressure drop at high space velocities [36]. In the steam reforming of biogas over Rh/CeO_2 on Al_2O_3 foams at high spatial velocities, like for other catalytic processes, the ppi modify the catalytic properties [38]. However, producing ceramic open-cell foams with high ppi and mechanical strength is challenging, instead metallic open-cell foams can be easily prepared.

A Ni foam was used to improve the heat transfer of a reactor for the combined steam-CO_2 reforming of methane, in the GTL-FPSO (gas to liquid-floating production storage and offloading) process [39], namely in a process where the same reactions as for the BSR are taking place. Consequently, a Ni/γ-Al_2O_3/Ni foam had a uniform temperature distribution along the catalyst-bed, the adhesion of the coating to the foam surface being of paramount importance. Moreover, a NiCrAl metal-foam coated by a 0.09 wt.% [Pd(7)–Rh(1)]/($CeZrO_2$–Al_2O_3) catalyst was compared with commercially available alumina-supported 8.0 wt.% Ru and 13.0 wt.% Ni catalysts for steam reforming of a model biogas [40].

Recently, we have studied the coating of high pore density NiCrAl open-cell foams by RhMgAl HT compounds by electrodeposition and after calcination at 900 °C, stable and active catalysts for the catalytic partial oxidation of CH_4 have been obtained [41]. Herein, we propose the intensification of the steam reforming of clean biogas process, at low S/C ratios, over Rh and Ru activated NiCrAl open-cell foams, prepared by electrodeposition of RhMgAl and RuMgAl compounds and calcination, also investigating the mechanism of carbon formation. Catalytic tests are performed at 5 bar to be closer to a real application and at high GHSV to highlight the differences among the different catalysts used [4].

2. Experimental part

2.1. Preparation of the catalysts

Chemicals used for the experiments include Rhodium (III) nitrate solution (~10% wt.% Rh in >5 wt.% HNO_3, Sigma Aldrich), Ruthenium (III) nitrosyl nitrate solution (Ru 1.5 wt.%, diluted in HNO_3, Alfa Aesar), Magnesium nitrate hexahydrate (Sigma Aldrich, 99%), Aluminum nitrate nonahydrate (Aldrich Sigma, 98%), and ammonia solution (25%, Merck). Structured support is a NiCrAl open-cell foam (disks in a dimension of 10 mm diameter x 1.6 mm thickness, 450 µm cell size) supplied by Alantum. Prior to coating, foam disks were pre-treated in HCl 1 M for 15 min, followed by rinsing thoroughly in ultra-pure water [41]. Then, M/Mg/Al (M = Rh or Ru) HT materials were in situ coated on the clean foam by electro-base generation technique in a double compartment electrochemical flow cell controlled by a potentiostat (Autolab, PGSTAT128N, Eco Chemie). Detailed information on the cell configuration can be found elsewhere [42]. Electrolytes are aqueous nitrate solutions (total concentration of 0.06 M) containing a mixture of cations $M^{3+}/Mg^{2+}/Al^{3+}$ (M^{3+} = Rh^{3+} or Ru^{3+}) with two different molar ratios of 5/70/25 and 2/70/28. The electrolyte was adjusted to pH 3.8, using a concentrated NH_4OH solution, to favor the deposition of a layer of HT material rather than the electro-reduction of noble metal cations to form metallic particles as reported elsewhere [43]. The coating process was performed at -1.2 V *vs* SCE (saturated calomel electrode) with an electrolyte flow of 2 mL min^{-1} for 2000 s for Rh-based samples as in our previous work [41] and 750 s for Ru-based samples. Note that the electrodeposition time applied for the Ru-based sample is adjusted, i.e. shortened to 750 s, to obtain a similar coating loading as for the Rh counterparts. The electrolyte containing the Ru nitrosyl complex favored the deposition process, hence a high rate of solid deposition was observed. Indeed, for the Ru-based electrolyte, a 2000 s synthesis led to deposit a large amount of coating causing almost the blockage of the foam pores. After being coated, the foams were rinsed thrice with ultra-pure water, dried at 40 °C for 24 h and then calcined in an oven at 900 °C (ramp 10 °C min^{-1}) for 12 h. The samples were denoted as Rh*x* (or Ru*x*) where *x* stands for molar ratios of Rh^{3+} (or Ru^{3+}) in the electrolytes. Note that the target of the electrodeposition is to obtain a layer of HT material containing noble metals that are

later transformed into mixed oxides during the calcination step and further reduced to nanoparticle size in the reduction step before the reaction.

For comparative purposes, a powder catalyst was prepared by the coprecipitation method. An aqueous nitrate solution containing a molar ratio of Rh/Mg/Al = 0.5/70/29.5 (Rh0.5) and total metal concentration of 1.0 M was dropped wise into a batch reactor containing 100 ml of a Na_2CO_3 solution under vigorous stirring at 60 °C. The pH was controlled at 10 ± 0.2 by adding dropwise a 1.0 M aqueous solution of NaOH. The amount of Na_2CO_3 was calculated by the charge balance of the system when a trivalent cation substituted a divalent one in the brucite structure with an excess amount of 50 %. The resulting slurry was aged for 0.5 h at 60 °C under stirring, filtered, and washed thoroughly with warm distilled water (60 °C). After filtration, the paste cake products were dried and subsequently calcined under the same conditions used for the foam catalysts.

2.2. Characterization techniques

Morphology of the coating was characterized by scanning electron microscopy (SEM) coupled to energy dispersive spectrometry (EDS) using an EP EVO 50 Series Instrument (EVO ZEISS) equipped with an INCA X-act Penta FET® Precision EDS microanalysis and INCA Microanalysis Suite Software (Oxford Instruments Analytical). The accelerating voltage was 20 kV and the spectra were collected in a duration of 60 s.

Porosity of the catalyst was determined by N_2 adsorption/desorption at -196 °C using a Micromeritics ASAP 2020 instrument. Due to the low amount of coating on the coated foam, each measurement was carried out with two calcined coated foams. Samples were degassed under vacuum (< 30 μm Hg) up to 250 ºC for 30 min. The specific surface area (S_{BET}) was calculated using the Brunauer-Emmett-Teller (BET) multiple-point method in the relative pressure range p/p^0 from 0.05 to 0.3.

Reduction property of the catalyst was studied by hydrogen temperature-programmed reduction (H_2-TPR) using an AutoChem II (Chemisorption analyzer, Micromeritics). The catalyst (two calcined coated foams) was activated at 150 ºC under 30 mL min^{-1} of He for 30 min. After cooling to 40 ºC under He, the carrier gas was switched to 5 % H_2/Ar (v/v) at 30 mL min^{-1}. When the baseline was stable, the temperature was increased to 950 ºC with a ramp of 10 ºC min^{-1}. The H_2 consumption was measured using a thermal conductivity detector (TCD).

High resolution transmission electron microscopy (HRTEM) characterization was carried out by a TEM/STEM FEI TECNAI F20 microscope, equipped with an EDS analyzer. The solid coating scratched from the foam catalysts was suspending in ethanol under ultrasounds for 20 min. The suspension was subsequently deposited on a Cu grid with lacey quanti-foil carbon film and dried at 100 ºC before doing the measurement. Selected area electron diffraction (SAED) and Fast Fourier transformation (FFT) were applied to determine the interplanar spacing of the crystals. Particle size distribution was processed considering around 150 particles in three different zones for each sample.

Micro-Raman measurements were performed in a Renishaw Raman Invia configured with a Leica DMLM microscope (obj. 5×, 20×, 50×). The available sources are an Ar^+ laser (514.5 nm, P_{max} = 30 mW) and a diode-laser (780.0 nm, P_{max} = 300 mW). The system was equipped with edge filters to cut Rayleigh scattering, monochromators (1800 lines/mm for Ar^+ laser, and 1200 lines/mm for diode laser) and a Charge-Coupled Device (CCD) thermoelectrically cooled (203 K) detector. Measurements were performed with the Ar^+ Laser (514.5 nm) at power level P_{out} = 3 mW (10% power). Each spectrum was recorded by four accumulations (30 s for each).

2.3. Catalytic tests

A tubular reactor (INCOLOY 800HT) with an internal diameter of 10 mm was loaded with four foam disks (10 mm diameter x 1.6 mm thickness) placed between two layers of inert material (quartz), and vertically placed into an electric tubular furnace. Catalysts were reduced in-situ before

catalytic tests with a continuous flow of H_2/N_2 (1/10 v/v, 200 mL min^{-1}) increasing the oven temperature from 30 to 900 °C (5°C min^{-1}) and holding this temperature for 1 h. Catalytic tests were carried out feeding a mixture of CH_4 (60% v/v) and CO_2 (40% v/v) regulated by thermal mass gas flow controllers. Water was pumped to the evaporator using an HPLC pump and the generated steam was mixed with the reaction mixture. The catalyst performance was evaluated at 5 bar by changing the temperature of the oven from 900 to 700 °C and using steam to methane ratios (S/CH_4) of the inlet stream of 1.0 and 0.5 (v/v). GHSV values of 30,000 and 40,000 h^{-1} were used (calculated on the total volume of the foam support at STP conditions) corresponding to values 8.0-13.5 • 10^5 mL h^{-1} g_{cat}^{-1} if the amount of deposited coating is considered. Reaction products were analysed on-line after water condensation by an Agilent Technology 7890A GC Gas chromatograph, equipped with two thermal conductivity detectors (TCD) and a CarboPLOT P7 column using H_2 for the CH_4, CO and CO_2 analyses and an HP-Molesieve column using N_2 for H_2 detection

A catalytic test using the Rh0.5 pelletized catalyst (fraction of particle sizes collected between the standard sieves of 30-40 mesh, 0.420-0.595 mm) was carried out at 900 ºC to compare with the results obtained over the Rh5 catalytic foams. Thus, 105 mg of Rh0.5 pelletized catalyst were loaded in the reactor maintaining the same amount of active phase as in the Rh5 experiment. Before catalytic tests, the catalyst was reduced under the same conditions as foam catalysts.

3. Results and discussion

3.1. Characterization of Rh and Ru structured catalysts

Electrodeposited films of nanoparticles of RhMgAl or RuMgAl HT precursors (Fig. 1a, 1b, Fig. S1a) generate, after calcination at 900 °C structured catalysts composed by a thin (ca. 15 μm) film of MgO and spinel phases coating the bumpy NiCrAl foam surface (Fig 1c, Fig. 1d, Fig. 2a, Fig. S1b). The morphology of the coatings and solid loadings (Table 1) are not largely affected by the composition of the deposited materials. This leads to rather similar specific surface area values,

around 2.3 – 2.6 $m^2\ g^{-1}$ or 45.1 – 51.1 $m^2\ g_{coating}^{-1}$, for all the catalysts (Table 1). Metallic loadings are 0.46 wt.% for Rh5, and 0.22 wt.% for Rh2 and Ru2 (referred to the total structured catalyst weight, Table 1). Rh easily disperses in the HT-derived catalyst even at high Rh loadings [44], while Ru can form segregated RuO_2 [45], however from SEM/EDS data, both elements seem to be well dispersed.

The structured catalysts are reduced during H_2-TPR experiments in a broad and high temperature range (Fig. 2b), note that the intensity of the signal is very low due to the small amount of catalyst. The reduction of Rh^{3+} and Ru^{4+} in HT-derived catalyst is expected to occur at 350-500 °C [43-45], the high temperatures are related to the interaction between noble metals and the oxide matrix, e.g. the Rh^{3+} could be inserted into the spinel forming a solid solution. However, in the structured catalysts here investigated, the interpretation of the reduction profiles is challenging. The peaks recorded in the reduction profiles are a combination of catalytic coating and support reduction. In fact, the calcined bare foam shows a peak centred at 480 °C attributed to the reduction of NiO. Moreover, it should be noted that noble metals promote the Ni^{2+} reduction and that a coating support interaction may occur. Namely, the formation of a $Mg_{1-x}Ni_xAl_2O_4$ solid solution may take place during calcination, and Ni^{2+} species in the spinel could be reduced in the high temperature range.

3.2. Steam reforming of clean biogas

After reduction at 900 °C, the catalysts have been tested in the steam reforming of biogas at P = 5 bar, investigating the effect of the reaction temperature and S/CH_4 ratio on the CH_4 and CO_2 conversions attained, and on the composition of the syngas produced. To know the thermodynamic limitations of the process at the operating conditions used, the equilibrium conversions of CH_4 and CO_2 were calculated using the software package Aspen HYSYS v8.4. In Table S1 the values obtained at 700, 800 and 900 ºC are shown. Furthermore, the influence of the temperature on the

equilibrium conversions of CH_4, CO_2 and H_2O, and on the H_2/CO ratio of the outlet stream for S/CH_4=1.0 and 0.5, respectively, are shown in Figs. S2a and S2b.

The increase of the reaction temperature reduces the differences between the experimental conversion and the maximum CH_4 and CO_2 conversions attainable at the thermodynamic equilibrium (Fig. 3a). This difference is also reduced increasing the S/CH_4 ratio. Thus, the most active catalyst, Rh5, achieves a CH_4 conversion of 88% at 900 ºC and S/CH_4=1.0, which represents the 90% of the maximum conversion possible, despite the high spatial velocity used in the test (GHSV= 40000 h^{-1}). The reduction of the number of active sites in Rh2 and Ru2 catalysts provokes a decrease in conversions; Rh2 is more active than Ru2, mainly in the CO_2 conversion. The high space velocity values used in this work were chosen to highlight the differences among the catalysts and actually, by decreasing the space velocity to 30,000 h^{-1}, both Rh2 and Ru2 increase the activity by around 10 % (Fig. S3). These results are particularly promising taking into account the low amount of catalyst loaded, indeed space velocities values calculated considering the mass of the catalyst are in the range of 8.0-13.5 • 10^5 mL h^{-1} g_{cat}^{-1}, at least an order of magnitude higher than those present in literature (Table S2).

The catalysts are still active in both steam and dry reforming at 800 °C, though the CO_2 conversion drops faster than CH_4 conversion. Contrarily, at 700 ºC, the equilibrium conversions of both CH_4 and CO_2 are still quite appreciable, but the experimental values are very low. Interestingly, the CO_2 conversion a S/CH_4=1.0 is negligible, see Fig. 3a, although the equilibrium conversion is around 48%. This means that the catalysts exert a kinetic control of the process, favoring the steam reforming instead of the dry reforming.

The syngas produced (Fig. 3b), regardless of the type of catalyst, has a H_2/CO ratio close to 2 at 900 and 800 °C and S/CH_4=1, i.e. when both steam and dry reforming and likely the Reverse Water Gas Shift (RWGS) reactions occur. However, H_2/CO ratio increases up to close 3 at 700 °C, because at this low-temperature dry reforming is minimized, and only steam reforming and Water

Gas Shift (WGS) occur. The tests at high space velocity indicate that the observed activity of the catalysts is promising, even for the low-loaded Rh2 catalyst. However, under these conditions, CH_4 is more prone to react with H_2O than with CO_2 [4,46] since H_2O is adsorbed in much higher extent than CO_2 and both of them compete for the same type of active sites [7]. Consequently, in the tests carried out at $S/CH_4 = 1.0$, around half of the CO_2 remains unreacted.

Under operation at lower steam content in the feed, i.e, $S/CH_4 = 0.5$ (Fig. 3a), it is observed that, at both 900 and 800 °C, CH_4 conversions decrease and CO_2 conversions increase, attaining comparable values for the three catalysts. In this case, the competition with adsorbed H_2O should be lower, hence CO_2 not only reacts with CH_4 through the dry reforming, but also with H_2 by the RWGS [7], as evidenced by the lower H_2/CO ratios (i.e. 1.5) of the syngas produced (Fig. 3b). Remarkably, the catalysts are active in the combined reforming even at low temperature (700 °C), though the production of CO_2 by the WGS, especially at $S/CH_4 = 1$ could be not negligible [5].

To make a comparison between the activity of the electrodeposited catalysts and those previously reported in the literature is not straightforward due to the differences in reaction conditions, mainly in the space velocity and volume of catalyst. Hence in Table S2, an estimation of the activities was made by comparing the amount of CH_4 and CO_2 converted per hour and gram of catalyst ($NL_{CH4,CO2}\ h^{-1}\ g_{cat}^{-1}$). Considering the data reported in Table S2, it can be stated that electrodeposited catalysts are promising for the reforming of biogas in comparison to both structured and powder catalysts reported in the literature.

The stability of the electrodeposited structured catalysts was investigated by performing a "control" test at T = 900 ºC, 30,000 h^{-1} and $S/CH_4 = 1$. Namely, after every series of tests performed at the different temperatures (900, 800, and 700 °C shown in Fig. 3a), the so-called "control" test was performed. The results are depicted in Fig. S3. CH_4 conversion remains rather stable, conversely, the CO_2 activation seems to improve during time-on-stream (TOS). To further investigate the stability of the three types of catalysts, a 6 h test was performed at 900 °C (40,000 h^{-}

^{1} and S/CH_4 = 1.0) at the end of each catalytic cycle (results not presented here). Rh-containing catalysts are the most stable with TOS exhibiting constant CH_4 conversion, for instance, 70 % for the Rh2 catalyst. However, the Ru2 catalyst steadily deactivates down to 39 % of conversion in CH_4. Lastly, the reproducibility and stability of the promising Rh2 catalyst were further assessed by loading new foams in the reactor and performing the tests at 900 °C (40,000 h^{-1} and S/CH_4 = 1.0) for 24 h TOS, including 4 shut-down and start-up cycles (cooling from reaction to room temperature and heating from room to reaction temperature under N_2 flow). The results are shown in Fig. 4. After a short activation period within the first 5 h TOS, only a slight decrease in the CH_4 conversion occurs, while CO_2 conversion oscillates in the 35-45% range. These results confirm the reproducibility and the resistance against the deactivation of this catalyst.

The catalytic results obtained in the reforming of clean biogas indicate that after an initial reaction period, wherein the activity is modified, Rh-containing catalysts are rather stable, showing high conversions of CH_4 (in the range of 80-90 % at 900 °C, S/CH_4=1.0, GHSV=30000 h^{-1}) and CO_2 (up to 71 % for Rh5 catalyst at 900 °C, S/CH_4=0.5, GHSV=40000 h^{-1}) despite the high space velocities used. The performance of the structured catalysts could be related to both the catalytic coating (i.e. stability of the catalytic layer and Rh metallic particles) and the NiCrAl foam support (e.g. enhancing mass and heat transfer).

Making a comparison between the performance of Rh5 structured catalyst and a pelletized catalyst at 900 °C in Fig. 5, it is evident that the structuration fosters the CH_4 conversion, while the effect on the CO_2 conversion depends on the S/CH_4 in the feedstock. At S/CH_4 = 1.0, the pelletized catalyst outperforms the structured one in CO_2 conversion, but the opposite is observed at S/CH_4 = 0.5. Note that the composition of the syngas is not significantly modified depending on the type of catalyst.

The enhanced activity of the structured catalyst, as above commented, could be related to the enhanced mass and heat transfer of the 3D support. However, the contribution of the metallic foam

support to the activity could not be ruled out. Ni, the main element in the NiCrAl alloy, is active in reforming reactions, moreover, in the H_2-TPR profile, it was observed that some Ni^{2+} is reduced (Fig. 2b). Actually, blank tests over pretreated and calcined bare foams, after reduction, confirm that the contribution of the foam to CH_4 and CO_2 activation is not negligible at 900 °C (Fig. S4). Note, however, that the activity quickly drops with TOS, more remarkably for the CO_2 conversion. These results suggest that the Ni is available to the reaction mixture (vide infra), contrarily to the behaviours observed for a Pd-Rh/$CeZrO_2$-Al_2O_3 catalyst coated on NiCrAl [40] and also by our group for similar Rh structured catalysts tested in the catalytic partial oxidation of CH_4 [41]. The differences can be related to the pretreatment of the foam before electrodeposition. Indeed, tests with a calcined bare foam do not show any remarkable activity in the reforming of biogas.

3.3. Characterization of spent catalysts

After the reaction, the foam pieces placed at different bed positions were characterized. The samples were labelled u1, u2, u3 and u4, where the numbers indicate the position in the catalytic bed, i.e. 1 at the inlet and 4 at the outlet (Fig. S5).

SEM images show that the coating is rather similar in spent than in fresh catalysts in terms of thickness and morphology; the main difference in the coating properties after the biogas reforming reaction is the development of large spherical particles (Fig. 6, Fig.s S6-S9). EDS analyses reveal that these particles are not made by Rh (or Ru), but contain Ni (and maybe Cr) coming from the support. Remarkably, segregated large particles are also observed in the spent pre-treated and calcined bare foams after catalytic tests (Fig. 6a1, Fig. S10), while they are not detected in the bare foams only calcined (not shown).

HRTEM images confirm that Rh spent catalysts contain two types of metallic particles that differ both in size and composition (Fig. 7, Fig. 8). A narrow and small Rh particle size distribution is embedded in or deposited on the MgO and $MgAl_2O_4$ matrix (Fig. 7a, 7b), characteristic of electrodeposited and coprecipitated HT-derived catalysts [41]. A strong metal support interaction

(SMSI) is evidenced (Fig. 7c), ensuring high stability of the Rh particles against thermal sintering. The Rh loading in the HT-derived catalysts slightly affects the size of this type of particles, a larger contribution of particles below 2 nm is observed for Rh2 than for Rh5 spent catalysts (Fig. 7b, 8b), however, it is tricky to give an accurate value of the Rh particle size distribution due to the formation of Ni or RhNi particles (vide infra). On the other hand, the position of the foam disk in the catalytic bed does not seem to play a crucial role in the properties of the particles. The second type of particles present in the spent catalysts are larger (Fig. 7a, 8a) and more importantly they are mainly made by Ni "doped" by Rh (Fig. 7e, 8c). Again, it is not straightforward to correlate the size of Ni-containing particles and the sintering since already a broad distribution of large particles is present in the reduced catalyst.

Taking into account the characterization of the calcined and spent catalysts, Ni from the foam is likely oxidized during the preparation of the structured catalyst; it could form free NiO or it could be included in the catalytic coating, e.g. as $Mg_{1-x}Ni_xAl_2O_4$. Both types of Ni species after reduction may form Ni metallic particles, and in some cases bimetallic RhNi particles (because of Rh-Ni interaction), which may contribute to the catalytic activity, e.g. the activation during the reaction. However, as above commented, the activity in the pre-treated calcined bare foam, containing large metallic particles, decreased with TOS. Hence, the contribution of the large Ni nanoparticles segregated from the metallic substrate to the activity may be very low (or negliglible). More detailed studies are required to better explain the role of Ni coming from the foam on the catalytic activity.

The presence of Ni, however, promotes carbon deposition [47]. Indeed, HRTEM images show that graphitic layers coat the surface of large Ni-containing particles, encapsulating carbon, and carbon nanotubes grow from Ni particles (Fig.7d, 8a). Though, it should be remarked that the amount of carbon probably is not very large. Carbonaceous deposits can be formed during the reaction, but they are reactive and may be partially removed from the catalyst by the effect of the

reverse Boudouard reaction, forming CO, or by gasification with steam. Unfortunately, in the present case, the results of the TGA experiments carried out are masked by the simultaneous and unavoidable Ni^0 oxidation. In addition, it was observed that some carbon formed is not well adhered to the foam surface and it is detached during handling.

To further investigate the carbon formation during the reaction, Raman spectra were recorded on different radial and axial positions along with the foam (Fig. 9). In Fig. S5 it is described the nomenclature used for the selected positions for the Raman measurements. The D band, around 1350 cm^{-1}, is related to the presence of defects on the carbonaceous materials formed during the reaction; while the G band, at 1580 cm^{-1}, is characteristic of well-defined graphitic and/or graphenic materials [48]. Therefore, a high value of the ratio I_G/I_D is usually associated with the formation of carbonaceous materials with a high graphitic character [48]. In Tables S3-S5 the I_G/I_D values obtained from the spectra of the foams after reaction at the different longitudinal and radial positions are summarized. The aim is to know if it is possible to detect any effect of the radial and longitudinal profiles of temperature and gas composition inside the foams, on the type of carbonaceous nanomaterials formed. From the results obtained, there is not a clear trend between the type of carbon formed and its position in the foam radius for all the investigated samples. These results can be explained considering that the high thermal conductivity of the metallic substrate of the foams avoids the presence of elevated gradients of temperature in the radial direction.

Considering the effect of the type of catalyst, Ru2 shows a lower carbon deposition, especially at the reactor inlet, in comparison with the Rh catalysts. For the Rh2 and Rh5 catalysts, the I_G/I_D ratio values calculated (Tables S3-S5) suggest the presence of both carbon nanotubes and amorphous carbon, along the whole catalytic bed, without a clear dependence with the longitudinal position. In the case of Ru2 catalyst, at the inlet position (u1), the formation of carbon is not detected, while in progressive positions the presence of carbon is common, see Table S3 and Fig. 9. Thus, in the exit position u4, the high I_G/I_D ratios measured indicate the development of a gradient

carbon concentration, which can be mainly assigned to the presence of highly graphitized carbon. In summary, Ru2 shows a lower carbon deposition, especially in positions close to reactor inlet, though it is the less stable catalyst; hence its deactivation could be related to modifications in the Ru particle size that need further investigation. On the other hand, on Rh catalysts (Rh5 and Rh2), the most resistant against deactivation catalysts, the formation of CNT and amorphous carbon along the reactor is higher. This fact confirms that carbon formation is mainly produced by the segregated Ni particles and it seems that it does not modify appreciably the reforming stability.

4. Conclusions

RuMgAl and RhMgAl structured catalysts based on NiCrAl open-cell foams, obtained by electrodeposition and calcination, are promising catalysts for the clean biogas steam reforming under flexible conditions. The structuration of the reactor allows operating at high space velocity values (in the order of $\approx 10^6$ mL h^{-1} g_{cat}^{-1}), minimizing the amount of catalyst loaded and attaining high mass and heat transfer rate in the harsh reaction conditions. At low S/CH_4 (i.e. 0.5) it is possible to increase the CO_2 conversion and the overall biogas valorisation. Rh catalysts exhibit higher activity and stability than Ru catalysts under all reaction conditions, outperforming the conventional Rh pelletized catalyst. Remarkably, the catalyst with a 0.22 wt.% Rh exhibits a high stability over 24 hour of time-on-stream at 900°C and $S/CH_4 = 1$ (GHSV = 10^6 mL h^{-1} g_{cat}^{-1}), even operating at transition conditions (i.e. 4 shut-down and start-up cycles). These excellent results are due to the formation of strong metal support interactions (SMSI) during reduction/reaction that stabilizes the catalytic sites and leads to the formation of highly active and well dispersed Rh nanoparticles. Moreover, the segregation of Ni from the NiCrAl support provoked the formation of large Rh/Ni and Ni metallic particles that, though active in the reaction, are the sites responsible for the deposition of carbonaceous nanomaterial (amorphous or CNT).

Acknowledgements

P. Tarifa acknowledges the financial support of Spanish Ministry (Ref.: BES-2014-069010). We acknowledge Alantum for supplying the metal foams.

References

[1] P. M. Mortensen, I. Dybkjær, Industrial scale experience on steam reforming of CO_2-rich gas, Appl. Catal. A: Gen. 495 (2015) 141–151.

[2] X. Zhao, B. Joseph, J. Kuhn, S. Ozcan, Biogas Reforming to Syngas: A Review, iScience, 23 (2020) 101082.

[3] G. A. Olah, A. Goeppert, M. Czaun, G. K. Surya Prakash, Bi-reforming of Methane from Any Source with Steam and Carbon Dioxide Exclusively to Metgas ($CO-2H_2$) for Methanol and Hydrocarbon Synthesis, J. Am. Chem. Soc. 135 (2013) 648–650.

[4] V. Chiodo, F. Urbani, A. Galvagno, N. Mondello, S. Freni, Analysis of biogas reforming process for molten carbonate fuel cells, J. Power Resources 206 (2012) 215–221.

[5] P. S. Roy, J. Song, K. Kim, C. S. Park, A. S. K. Raju, CO_2 conversion to syngas through the steam-biogas reforming process, J. CO_2 Utiliz. 25 (2018) 275–282.

[6] P. Kolbitsch, C. Pfeifer, H. Hofbauer, Catalytic steam reforming of model biogas, Fuel 87 (2008) 701–706.

[7] N. Guilhaume, D. Bianchi, R. A. Wandawa, W. Yin, Y. Schuurman, Study of CO_2 and H_2O adsorption competition in the combined dry/steam reforming of biogas, Catal. Today, Article in press https://doi.org/10.1016/j.cattod.2020.04.058

[8] K. Jabbour, P. Massiani, A. Davidson, S. Casale, N. El Hassan, Ordered mesoporous “one-pot” synthesized Ni-Mg(Ca)-Al_2O_3 as effective and remarkably stable catalysts for combined steam and dry reforming of methane (CSDRM), Appl. Catal. B: Environ. 201 (2017) 527–542.

[9] M. M. Danilova, Z. A. Fedorova, V. I. Zaikovskii, A. V. Porsin, V. A. Kirillov, T. A. Krieger, Porous nickel-based catalysts for combined steam and carbon dioxide reforming of methane, Appl. Catal. B: Environ. 147 (2014) 858–863

[10] F. Meshkani, M. Rezaei, M. Andache, Investigation of the catalytic performance of Ni/MgO catalysts in partial oxidation, dry reforming and combined reforming of methane, J. Ind. Eng. Chem. 20 (2014) 1251–1260

[11] T. Ohi, T. Miyata, D. Li, T. Shishido, T. Kawabata, T.Sano, K. Takehira, Sustainability of Ni loaded Mg–Al mixed oxide catalyst in daily startup and shutdown operations of CH_4 steam reforming, Appl. Catal. A: Gen. 308 (2006) 194–203.

[12] C. Liu, J. Ye, J. Jiang, Y. Pan, Progresses in the preparation of Coke Resistant Ni-based Catalyst for Steam and CO_2 Reforming of Methane, ChetCamChem 3 (2011) 529–541.

[13] S. D. Angeli, L. Turchetti, G. Monteleone. A. A. Lemonidou. Catalyst development for steam reforming of ethane and model biogas at low temperature, Appl. Catal. B: Environ. 181 (2016) 34–36.

[14] V. V. Kuznetsov, O. V. Vitovskii, O. A. Gasenko, Steam Reforming of Biogas over Rh/Al_2O_3 Catalyst in an Annular Microreactor, Theor. Found. Chem. Eng. 48 (2014) 376–381.

[15] M. A Soria, C. Mateos-Pedrero, A. Guerrero-Ruiz, I. Rodrìguez-Ramos, Thermodynamic and experimental study of combined dry and steam reforming of methane on Ru/ ZrO_2-La_2O_3 catalyst at low temperature, Int. J. Hydrog. Energy 36 (2011) 15212–15220.

[16] D. G. Avraam, T. I. Halkides, D. K. Liguras, O. A. Bereketidou, M. A. Goula, An experimental and theoretical approach for the biogas steam reforming reaction, Int. J. Hydrog. Energy 35 (2010) 9818–9827.

[17] Y. Khani, Z. Shariatinia, F. Bahadoran, High catalytic activity and stability of $ZnLaAlO_4$ supported Ni, Pt and Ru nanocatalysts applied in the dry, steam and combined dry-steam reforming of methane, Chem. Eng. J. 299 (2016) 353–366.

[18] A. Alvarez M, M. A. Centeno, J. A. Odriozola, Ru–Ni Catalyst in the Combined Dry-Steam Reforming of Methane: The Importance in the Metal Order Addition, Top. Catal. 59 (2016) 303–313.

[19] I. Luisetto, C. Sarno, D. De Felicis, F. Basoli, C. Battocchio, S. Tuti, S. Licoccia, E. Di Bartolomeo, Ni supported on γ-Al_2O_3 promoted by Ru for the dry reforming of methane in packed and monolithic reactors, Fuel Process. Technol. 158 (2017) 130–140.

[20] H. Zhou, T. Zhang, Z. Sui, Y. A. Zhu, C. Han, K. Zhu, X. Zhou, A single source method to generate Ru-Ni-MgO catalysts for methane dry reforming and the kinetic effect of Ru on carbon deposition and gasification, Appl. Catal. B: Environ. 233 (2018) 143–159.

[21] M. Garcìa-Diéguez, I. S. Pieta, M. C. Herrera, M. A. Larrubia, L. J. Alemany, RhNi nanocatalysts for the CO2 and CO_2 + H_2O reforming of methane, Catal. Today 172 (2011) 136–142.

[22] U. Izquierdo, V. L. Barrio, K. Bizkarra, A. M. Gutierrez, J. R. Arraibi, L. Gartzia, J. Banuelos, I. Lopez-Arbeloa, J. F. Cambra, Ni and Rh/Ni catalysts supported on Zeolites L for hydrogen and syngas production by biogas reforming processes, Chem. Eng. J. 238 (2014) 178–188.

[23] S. Ketheria, G. Deo, D. Kunzru, Rh-Ni/$MgAl_2O_4$ catalyst for steam reforming of methane: Effect of Rh doping, calcination temperature and its application on metal monoliths, Appl. Catal. A: Gen. 570 (2019) 308–318.

[24] I. H. Son, S. J. Lee, A. Soon, H.S. Roh, H. Lee, Steam treatment on Ni/γ-Al_2O_3 for enhanced carbon resistance in combined steam and carbon dioxide reforming of methane, Appl. Catal. B: Environ. 134-135 (2013) 103–109.

[25] A. Wolfbeisser, O. Sophiphun, J. Bernardi, J. Wittayakun, K. Fottinger, G. Rupprechter, Methane dry reforming over ceria-zirconia supported Ni catalysts, Catal. Today 277 (2016) 234–245.

[26] D. B. L. Santos, F. B. Noronha, C. E. Hori, Bi-reforming of methane for hydrogen production using $LaNiO_3$/$Ce_xZr_{1-x}O_2$ as precursor material, Int. J. Hydrog. Enery 45 (2020) 13947–13959.

[27] N. D. Charisiou, G. Siakavelas, K. N. Papageridis, A. Baklavaridis, L. Tzounis, D. G. Avraam, M. A. Goula, Syngas production via the biogas dry reforming reaction over nickel supported on modified with CeO_2 and/or La_2O_3 alumina catalysts, J. Nat. Gas Sci. Eng. 31 (2016) 164–183

[28] H. S. Roh, K. Y. Koo, J. H. Jeong, Y. T. Seo, D. J. Seo, Y. S. Seo, W. L. Yoon, S. B. Park, Combined reforming of methane over supported Ni catalysts, Catal. Lett. 117 (2007) 85–90.

[29] B. Huang, X. Li, S. Ji, B. Lang, F. Habimana, C. Li, Effect of MgO promoter on Ni-based SBA-15 catalysts for combined steam and carbon dioxide reforming of methane, J. Nat. Gas Chem. 17 (2008) 225–231.

[30] J. L. Ewbank, L- Kovarik, F. Z. Diallo, C. Sievers, Effect of metal–support interactions in Ni/Al2O3catalysts with low metal loading for methane dry reforming, Appl. Catal. A: Gen. 494 (2015) 57–67.

[31] L Zhang, X. Wang, C. Chen, X. Zou, W. Ding, X. Lu, Dry reforming of methane to syngas over lanthanum-modified mesoporous nickel aluminate/g-alumina nanocomposites by one-pot synthesis, Int. J. Hydrog. Energy 42 (2017) 11333-11345.

[32] N. Schiaroli, C. Lucarelli, G. Sanghez de Luna, G. Fornasari, A. Vaccari, Ni-based catalysts to produce synthesis gas by combined reforming of clean biogas, Appl. Catal. A: Gen. 582 (2019) 117087–117099.

[33] A. L. A. Marinho, R. C. Rabelo-Neto, F. Epron, N. Bion, F. S. Toniolo, F. B. Noronha, Embedded Ni nanoparticles in $CeZrO_2$ as stable catalyst for dry reforming of methane, Appl. Catal. B: Environ. 268 (2020) 118387.

[34] A. V. P. Lino, E. M. Assaf, J. M. Assaf, Hydrotalcites derived catalysts for syngas production from biogas reforming: Effect of nickel and cerium load, Catal. Today 289 (2017) 78–88.

[35] D. Y. Kalai, K. Stangeland, W. M. Tucho, Y. Jin, Z. Yu, Biogas reforming on hydrotalcite-derived Ni-Mg-Al catalysts: the effect of Ni loading and Ce promotion, J. CO_2 Utiliz. 33 (2019) 189–200.

[36] E. Tronconi, G. Groppi, C. G. Visconti, Structured catalysts for non-adiabatic applications. Curr. Opin. Chem. Eng. 5 (2014) 55–67.

[37] C. Italiano, R. Balzarotti, A. Vita, S. Latorrata, C. Fabiano, L. Pino, C. Cristiani, Preparation of structured catalysts with Ni and Ni–Rh/CeO_2 catalytic layers for syngas production by biogas reforming processes, Catal. Today 273 (2016) 3–11.

[38] C. Italiano, M. A. Ashraf, L. Pino, C. W. Moncada Quintero, S. Specchia, A. Vita, Rh/CeO_2 Thin Catalytic Layer Deposition on Alumina Foams: Catalytic Performance and Controlling Regimes in Biogas Reforming Processes, Catalysts 8 (2018) 448.

[39] D. Park, D. J. Moon, T. Kim, Preparation and evaluation of a metallic foam catalyst for steam-CO_2 reforming of methane in GTL-FPSO process, Fuel Process. Technol. 124 (2014) 97–103.

[40] P. S. Roy, C. S. Parka, A. S. K. Raju, K. Kim, Steam-biogas reforming over a metal-foam-coated (Pd–Rh)/($CeZrO_2$ –Al_2O_3) catalyst compared with pellet type alumina-supported Ru and Ni catalysts, J. CO_2 Utiliz. 12 (2015) 12–20.

[41] P. H. Ho, W. de Nolf, F. Ospitali, D. Beton, L. Torkuhl, G. Fornasari, A. Vaccari, P. Benito, Insights into coated NiCrAl open-cell foams for the catalytic partial oxidation of CH_4, React. Chem. Eng. 4 (2019) 1768−1778.

[42] P. H. Ho, W. de Nolf, F. Ospitali, A. Gondolini, G. Fornasari, E. Scavetta, D. Tonelli, A. Vaccari, P. Benito, Coprecipitated-like hydrotalcite-derived coatings on open-cell metallic foams by electrodeposition: Rh nanoparticles on oxide layers stable under harsh reaction conditions. Appl. Catal. A Gen. 560 (2018) 12−20.

[43] F. Basile, P. Benito, G. Fornasari, M. Monti, E. Scavetta, D. Tonelli, A. Vaccari, Novel Rh-based structured catalysts for the catalytic partial oxidation of methane, Catal. Today 157 (2010) 183−190.

[44] F. Basile, P. Benito, G. Fornasari, A. Vaccari, Hydrotalcite-type precursors of active catalysts for hydrogen production, Appl. Clay Sci. 48 (2010) 250−259.

[45] A. Ballarini, P. Benito, G. Fornasari, O. Scelza, A. Vaccari, Role of the composition and preparation method in the activity of hydrotalcite-derived Ru catalysts in the catalytic partial oxidation of methane, Int. J. Hydrog. Energy 38 (2013) 15128−15139.

[46] D. Papurello, V. Chiodo, S. Maisano, A. Lanzini, M. Santarelli, Catalytic stability of a Ni-Catalyst towards biogas reforming in the presence of deactivating trace compounds, Renew. Energy 127 (2018) 481−494.

[47] J. Sehested, Four challenges for nickel steam-reforming catalysts, Catal. Today 111 (2006) 103-110.

[48] A.C. Ferrari and D.M. Basko, Raman spectroscopy as a versatile tool for studying the properties of graphene; Nature Nanotech. 8 (2013) 235-246.

Supporting Information

Pilar Tarifa,[1,2,§] Nicola Schiaroli,[1,§] Phuoc Hoang Ho,[1,†] Fernando Cañaza,[2] Francesca Ospitali,[1] Giancosimo Sanghez de Luna,[1] Carlo Lucarelli,[3] Giuseppe Fornasari,[1] Angelo Vaccari,[1] Antonio Monzon,[2] Patricia Benito[1,*]

[1]Dipartimento di Chimica Industriale "Toso Montanari", Viale Risorgimento 4, 40136, Bologna, Italy

[2]Instituto de Nanociencia y Materiales de Aragón-INMA, (CSIC-University of Zaragoza), Zaragoza (Spain)

[3]Dipartimento di Scienza e Alta tecnologia, via Valleggio 9, 22100, Como, Italy

§ P. Tarifa and N. Schiaroli contributed equally

[†]Present address: Chemical Engineering, Competence Centre for Catalysis, Chalmers University of Technology, SE-412 96 Gothenburg, Sweden

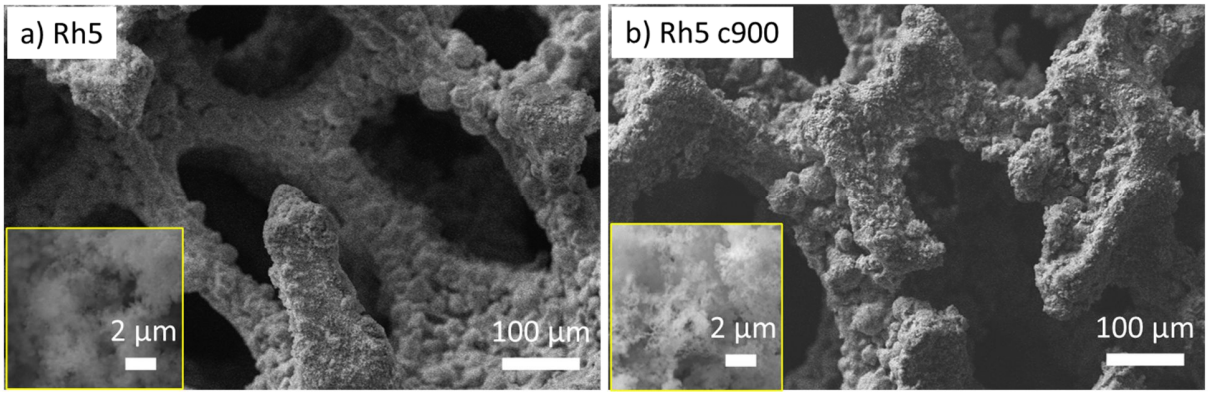

Fig. S1. SEM images of electrodeposited (a) and calcined Rh5 catalysts (b).

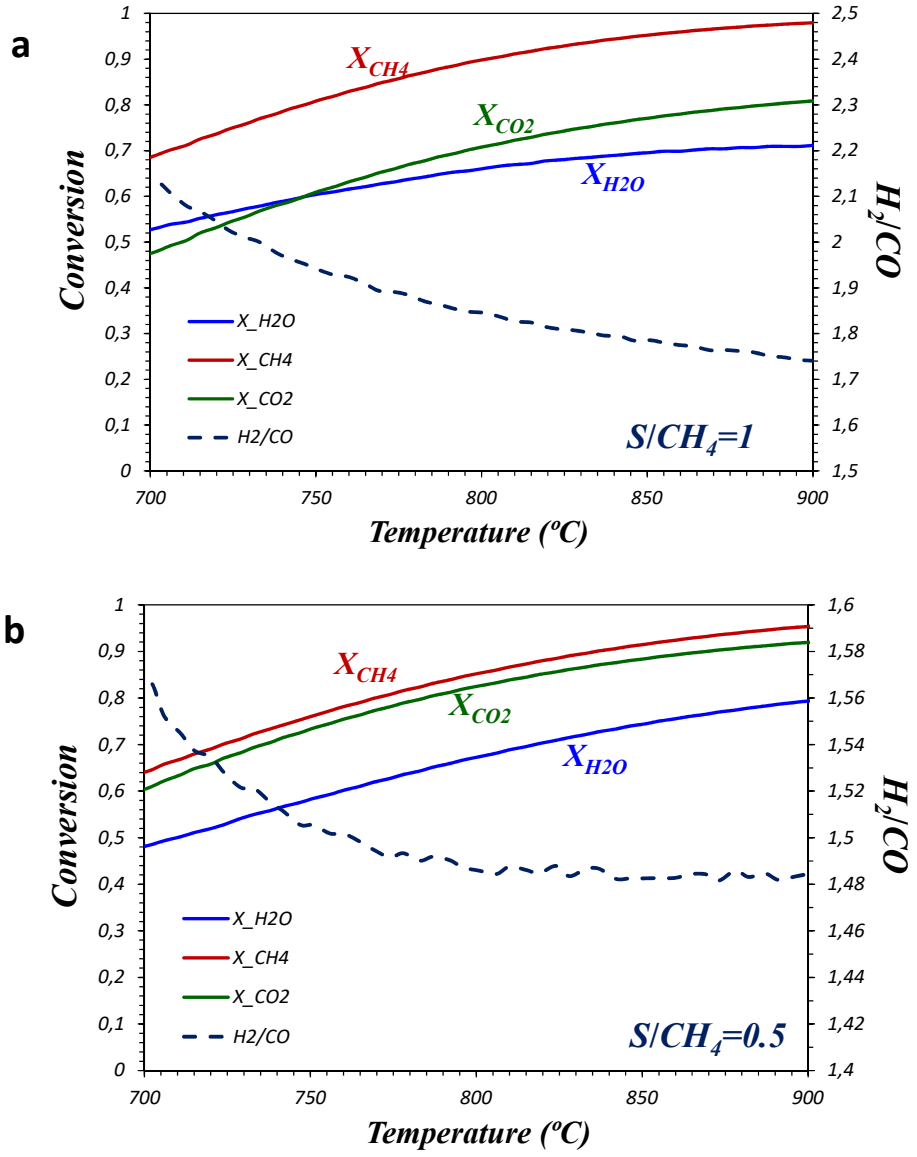

Fig. S2. Equilibrium conversions and related H_2/CO ratio at S/CH_4= 0.5 (a) and S/CH_4= 1 (b).

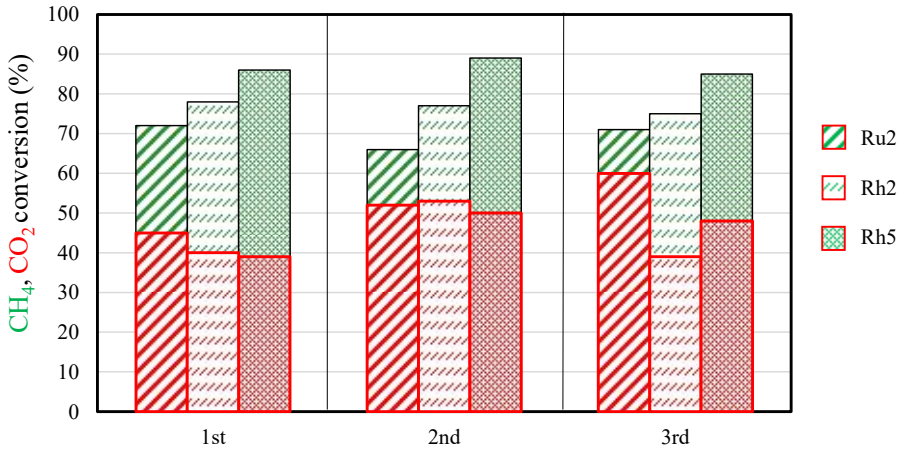

Fig. S3. Conversion of CH_4 and CO_2 during 3 cycles of the deactivation tests, T: 900 °C, S/CH_4: 1, GHSV: 30000 h^{-1}. 1st, 2nd and 3rd are the "control tests" performed after every series of catalytic tests carried out at 900, 800 and 700°C respectively.

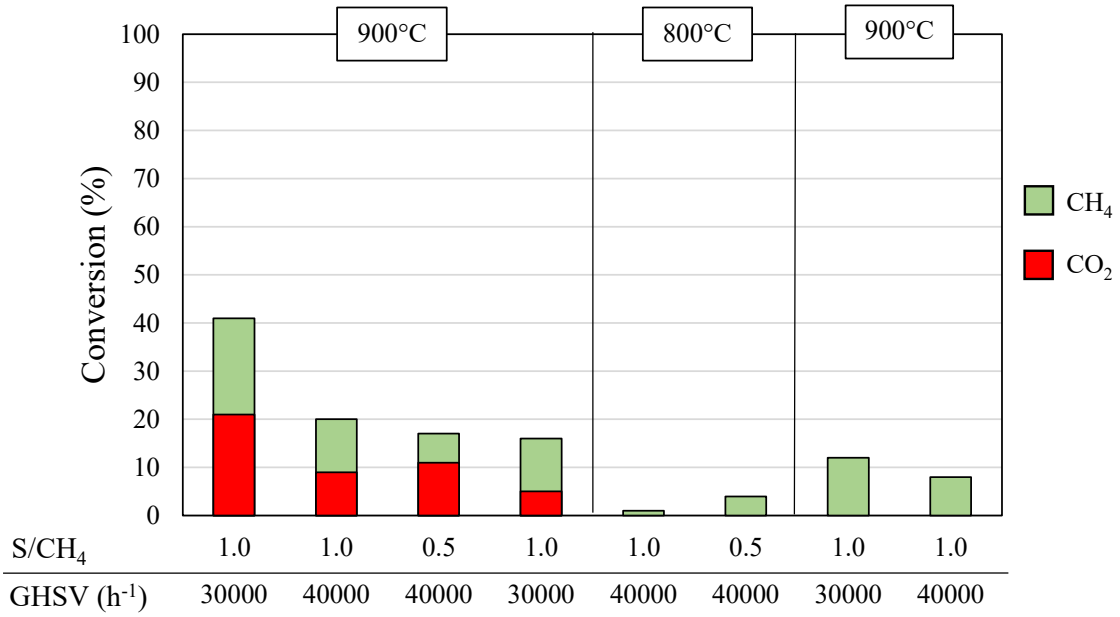

Fig. S4. Activity of the pretreated bare foam calcined at 900 °C. Reaction conditions: T= 900 and 800 °C; S/CH_4 = 1.0 and 0.5; GHSV = 30000 and 40000 h^{-1}. The tests are ordered by chronological order moving from the left to the right of the graph.

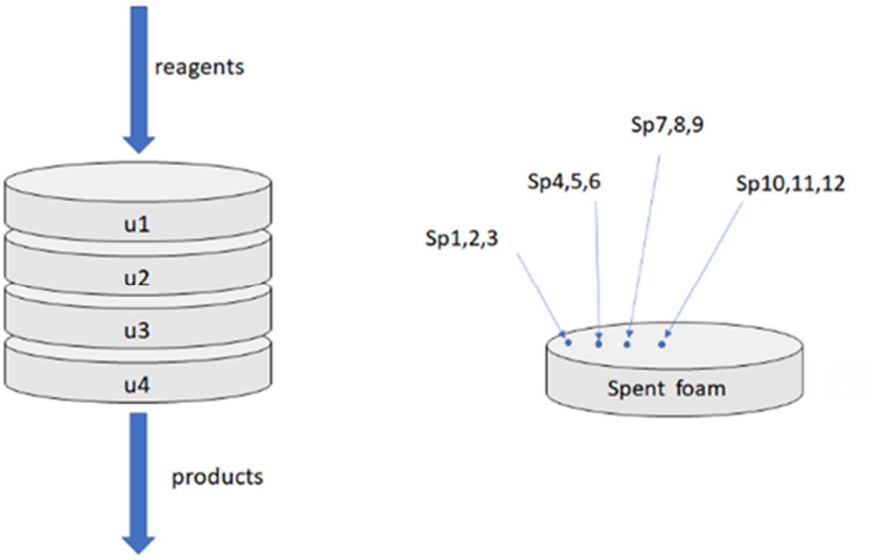

Fig. S5. Longitudinal (u1 to u4) and axial (1 to 12) positions of the Raman measurements.

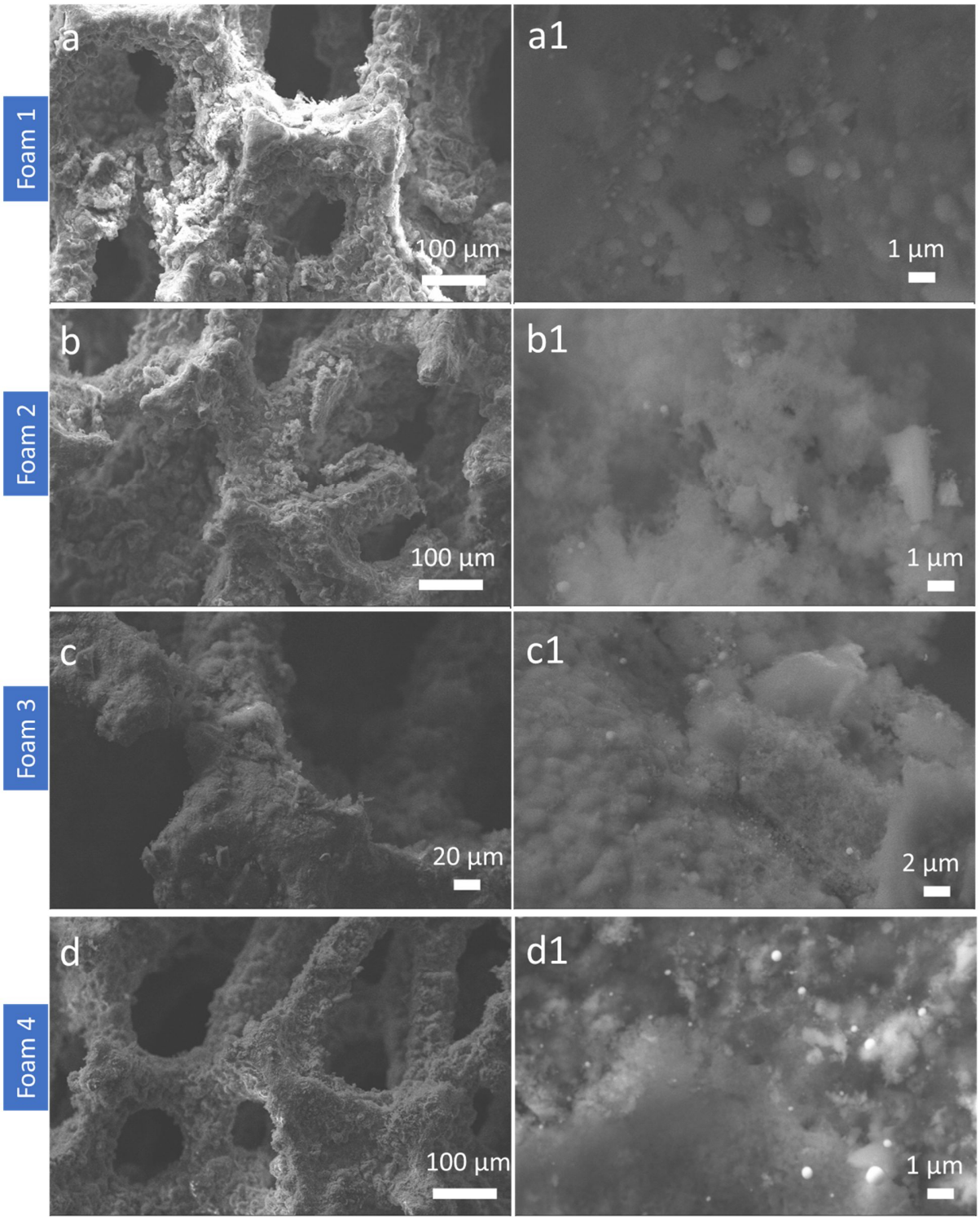

Fig. S6. SEM images of four foams of Rh5 catalyst after the catalytic tests. Foam 1 is the foam at the inlet and Foam 4 at the outlet of the catalytic bed.

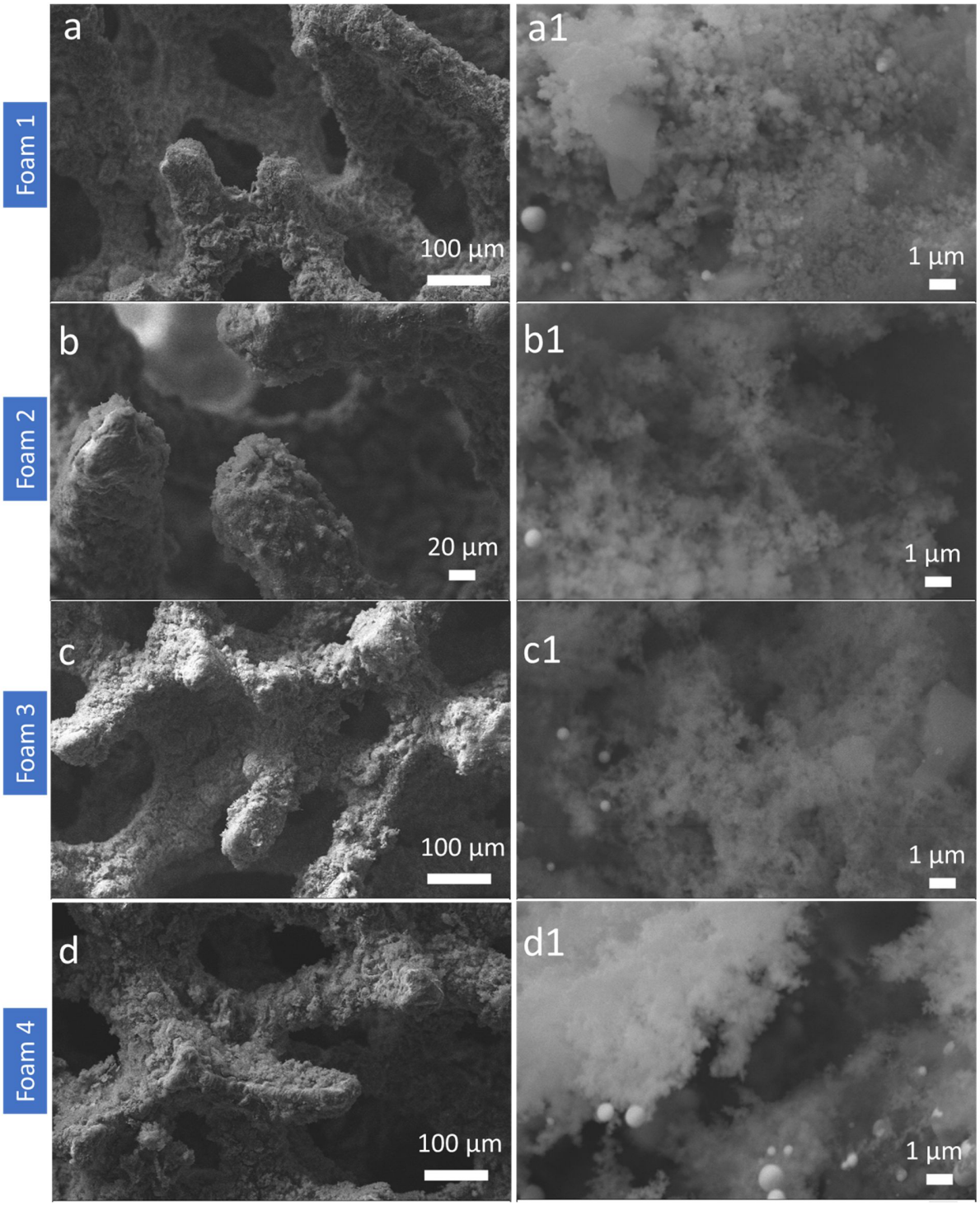

Fig. S7. SEM images of four foams of Rh2 catalyst after the catalytic tests. Foam 1 is the foam at the inlet and Foam 4 at the outlet of the catalytic bed.

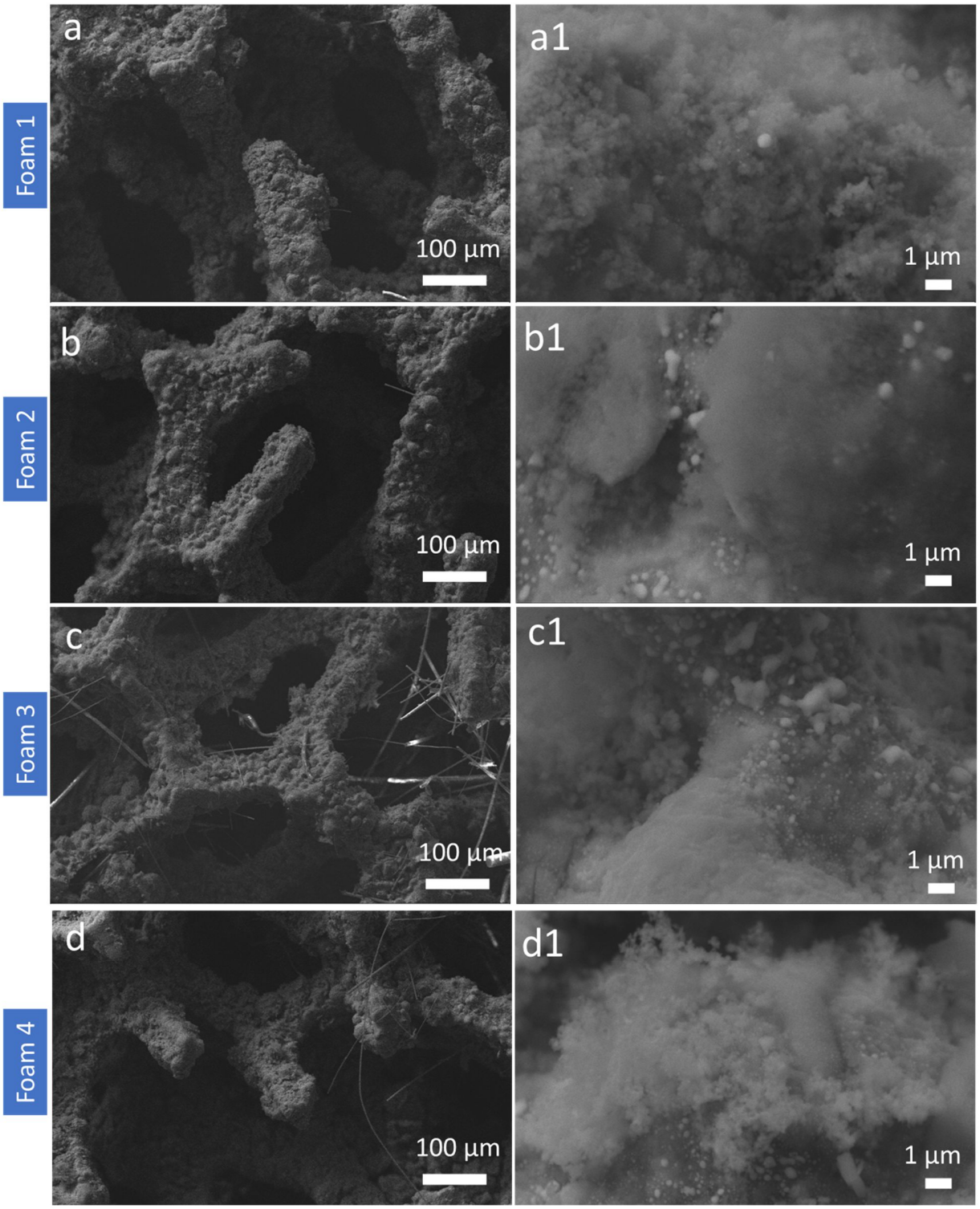

Fig. S8. SEM images of four foams of Rh2 catalyst after the 24h-stability test. Foam 1 is the foam at the inlet and Foam 4 at the outlet of the catalytic bed.

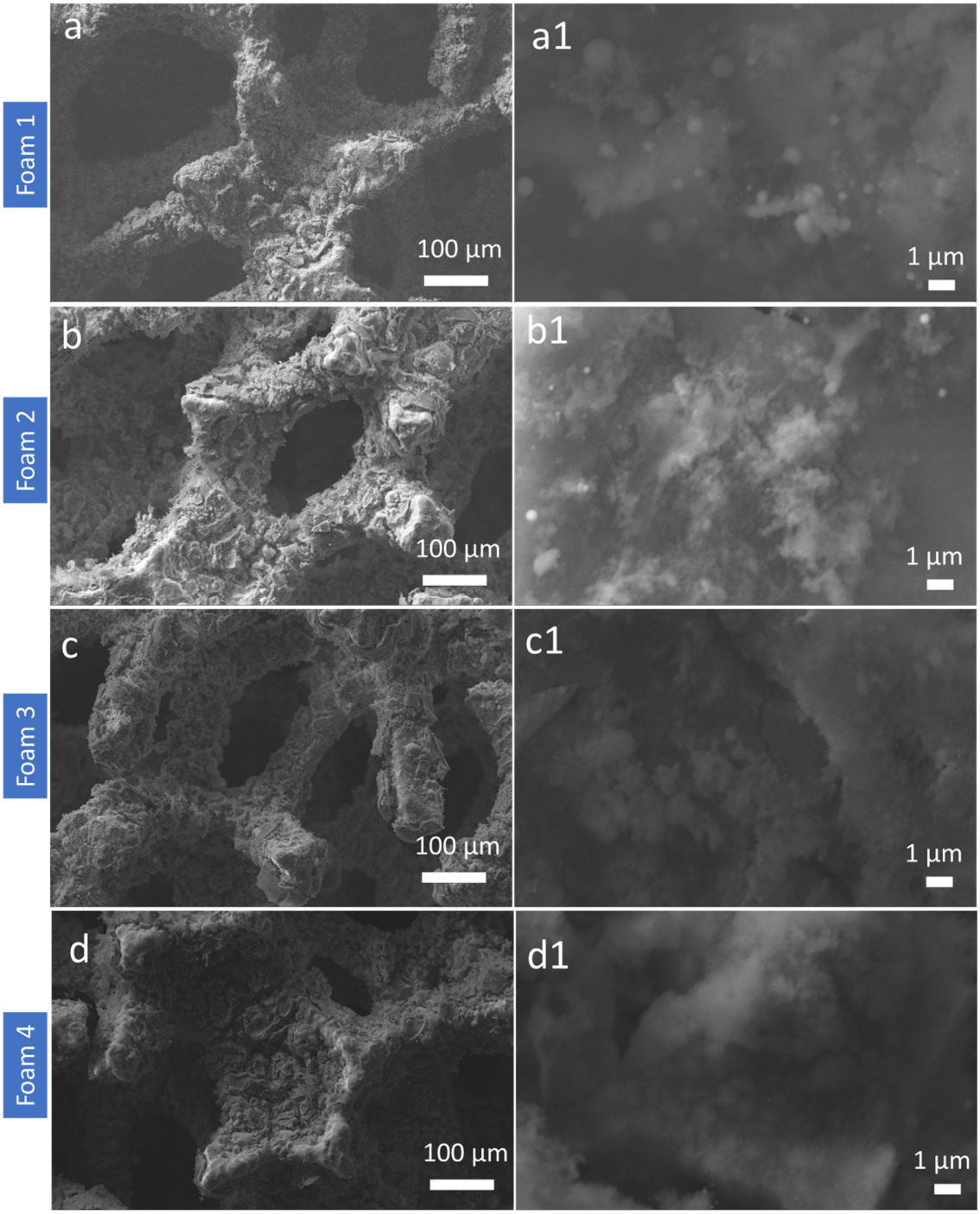

Fig. S9. SEM images of four foams of Ru2 catalyst after the catalytic tests. Foam 1 is the foam at the inlet and Foam 4 at the outlet of the catalytic bed.

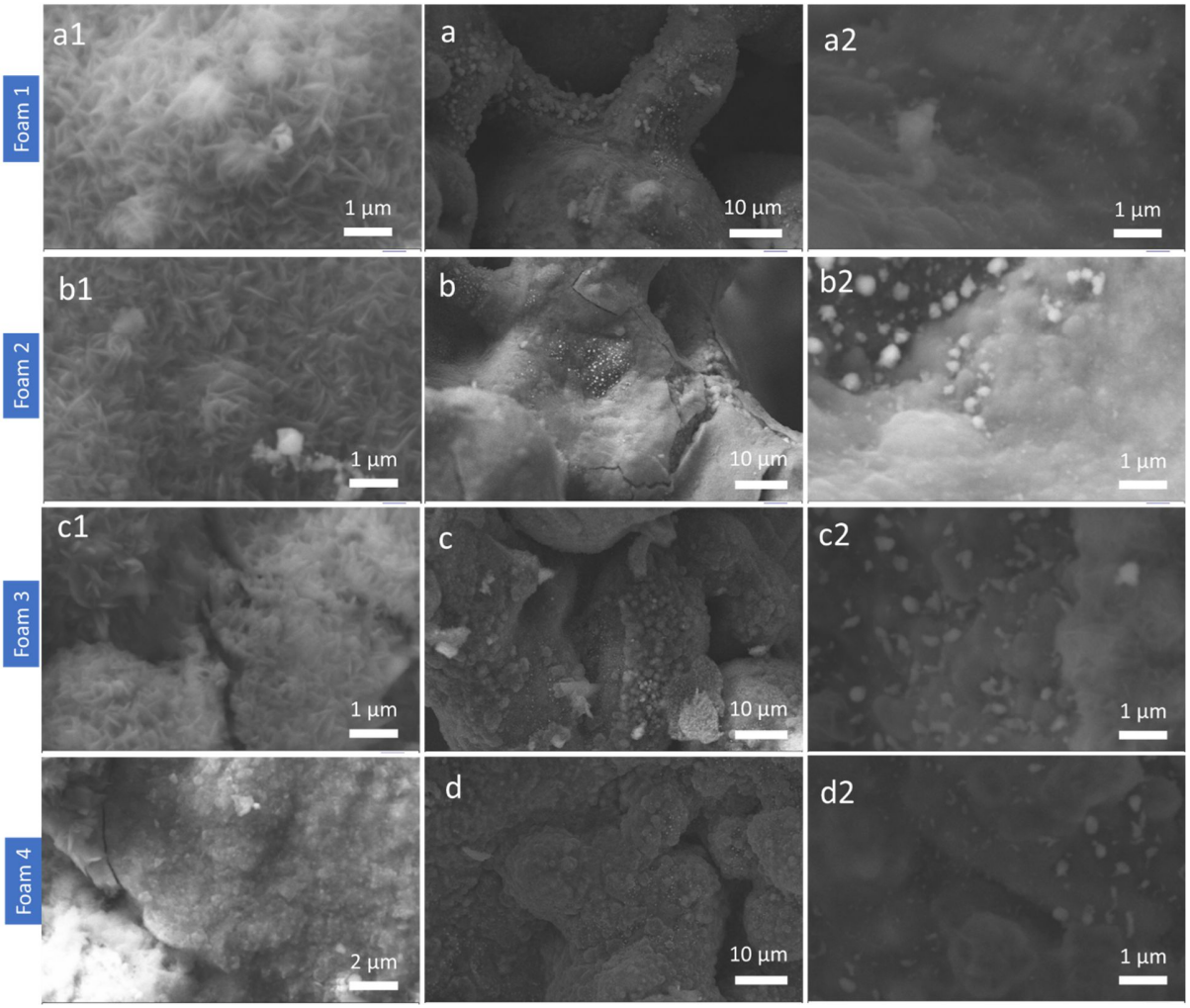

Fig. S10. SEM images of four bare foams (treated in HCl) after the catalytic test. Foam 1 is the foam at the inlet and Foam 4 at the outlet of the catalytic bed.

Table S1. Equilibrium conversion of CH_4 and CO_2 at the studied conditions, P=5 bar.

Temp. (°C)	$X_{CH4,\ equil.}$	$X_{CO2,\ equil.}$	$H_2/CO_{,\ equil.}$	***S/CH₄***
700	0.68	0.48	2.14	1
800	0.90	0.71	1.85	
900	0.98	0.81	1.74	
700	0.64	0.60	1.57	0.5
800	0.85	0.83	1.49	
900	0.95	0.92	1.48	

Table S2. Comparison between some literature results and that obtained in this work.

Catalyst	T / °C	P / MPa	S/CH_4/ v/v	GHSV / mL h^{-1} g^{-1}	CH_4 converted/ NL h^{-1} g^{-1}	CO_2 converted/ NL h^{-1} g^{-1}	ref
Rh5	900	0.5	1.00	1,010,738	326	99	This work
	900	0.5	1.00	1,353,020	446	159	This work
	900	0.5	0.50	1,353,020	474	294	This work
	800	0.5	1.00	1,353,020	294	71	This work
	800	0.5	0.50	1,353,020	287	145	This work
	700	0.5	1.00	1,353,020	142	-17	This work
	700	0.5	0.50	1,353,020	125	21	This work
Rh/CeO_2	900	0.1	1.00	72,000	21.6	9.4	Vita [1]
$Ni-Rh/CeO_2$	800	0.1	1.00	72,000	14.8	6.4	Italiano [2]
Ru-Ni/MgAl	750	0.1	0.56	120,000	33.7	13.5	Alvarez[3]
$Ni-La/SiO_2$	830	0.1	0.80	158,400	69.1	23.0	Chen [4]
Ni/Al_2O_3	800	0.1	0.80	69,000	4.0	1.6	Jabbour[5]
Ni/Mg/SBA	850	0.1	0.50	27,000	11.8	8.3	Huang [6]
$Ru/LaZnAlO_4$	800	0.1	0.75	12,000	5.0	1.6	Khani [7]
$LaNiO_3/Ce_{0.75}Zr_{0.25}O_2$	800	0.1	0.67	125,000	50.0	12.5	Santos [8]
$Rh-Ni/Al_2O_3$	700	0.1	0.65	29,880	3.6	1.5	Dieguez [9]

References for data in Table S2.

[1] A. Vita, C. Italiano, M. A. Ashraf, L. Pino, S. Specchia, Syngas production by steam and oxy-steam reforming of biogas on monolith-supported CeO_2-based catalysts, Int. J. Hydrog. Energy 43 (2018) 11731-11744.

[2] C. Italiano, R. Balzarotti, A. Vita, S. Latorrata, C. Fabiano, L. Pino, C. Cristiani, Preparation of structured catalysts with Ni and Ni–Rh/CeO2 catalytic layers for syngas production by biogas reforming processes, Catal. Today 273 (2016) 3–11.

[3] A. Alvarez M, M. A. Centeno, J. A. Odriozola, Ru–Ni Catalyst in the Combined Dry-Steam Reforming of Methane: The Importance in the Metal Order Addition, Top. Catal. 59 (2016) 303-313.

[4] C. Chen, X. Wang, X. Chen, X. Liang, X. Zou, X. Lu, Combined steam and CO2 reforming of methane over one-pot prepared Ni/La-Si catalysts, Int. J. Hydrog. Energy 44 (2019) 4780-4793.

[5] K. Jabbour, P. Massiani, A. Davidson, S. Casale, N. El Hassan, Ordered mesoporous “one-pot” synthesized Ni-Mg(Ca)-Al_2O_3 as effective and remarkably stable catalysts for combined steam and dry reforming of methane (CSDRM), Appl. Catal. B Environ. 201 (2017) 527-542

[6] B. Huang, X. Li, S. Ji, B. Lang, F. Habimana, C. Li, Effect of MgO promoter on Ni-based SBA-15 catalysts for combined steam and carbon dioxide reforming of methane, J. Nat. Gas Chem. 17 (2008) 225-231.

[7] Y. Khani, Z. Shariatinia, F. Bahadoran, High catalytic activity and stability of $ZnLaAlO_4$ supported Ni, Pt and Ru nanocatalysts applied in the dry, steam and combined dry-steam reforming of methane, Chem. Eng. J. 299 (2016) 353-366.

[8] D. B. L. Santos, F. B. Noronha, C. E. Hori, Bi-reforming of methane for hydrogen production using $LaNiO_3/CexZr_{1-x}O_2$ as precursor material, Int. J. Hydrog. Energy 45 (2020) 13947-13959.

[9] M. García-Diéguez, I. S. Pieta, M. C. Herrera, M. A. Larrubia, L. J. Alemany, RhNi nanocatalysts for the CO_2 and $CO_2 + H_2O$ reforming of methane, Catal. Today 172 (2011) 136-142.

Table S3. Raman results obtained with the Ru2 foams after reaction. Effect of longitudinal and radial positions on the I_G/I_D ratios (see Figure 9 and S5).

Radius foam

Gas flow

u1

Spot	I_G/I_D	Spot	I_G/I_D	Spot	I_G/I_D	Spot	I_G/I_D
1	No Spot	4	-	7	-	10	No Spot
2	-	5	-	8	-	11	No Spot
3	2,83	6	-	9	-	12	No Spot

u2

Spot	I_G/I_D	Spot	I_G/I_D	Spot	I_G/I_D	Spot	I_G/I_D
1	-	4	-	7	0,54	10	-
2	0,94	5	-	8	0,87	11	-
3	-	6	-	9	0,45	12	0,75

u3

Spot	I_G/I_D	Spot	I_G/I_D	Spot	I_G/I_D	Spot	I_G/I_D
1	10,55	4	24,15	7	9,17	10	10,77
2	7,25	5	9,66	8	5,20	11	6,20
3	-	6	7,19	9	1,18	12	1,25

u4

Spot	I_G/I_D	Spot	I_G/I_D	Sp	I_G/I_D	Spot	I_G/I_D
1	12,13	4	12,27	7	18,77	10	15,79
2	15,33	5	1,69	8	14,60	11	13,55
3	20,69	6	1,23	9	-	12	-

Table S4. Raman results obtained with the Rh2 foams after reaction. Effect of longitudinal and radial positions on the I_G/I_D ratios (see Figure S5).

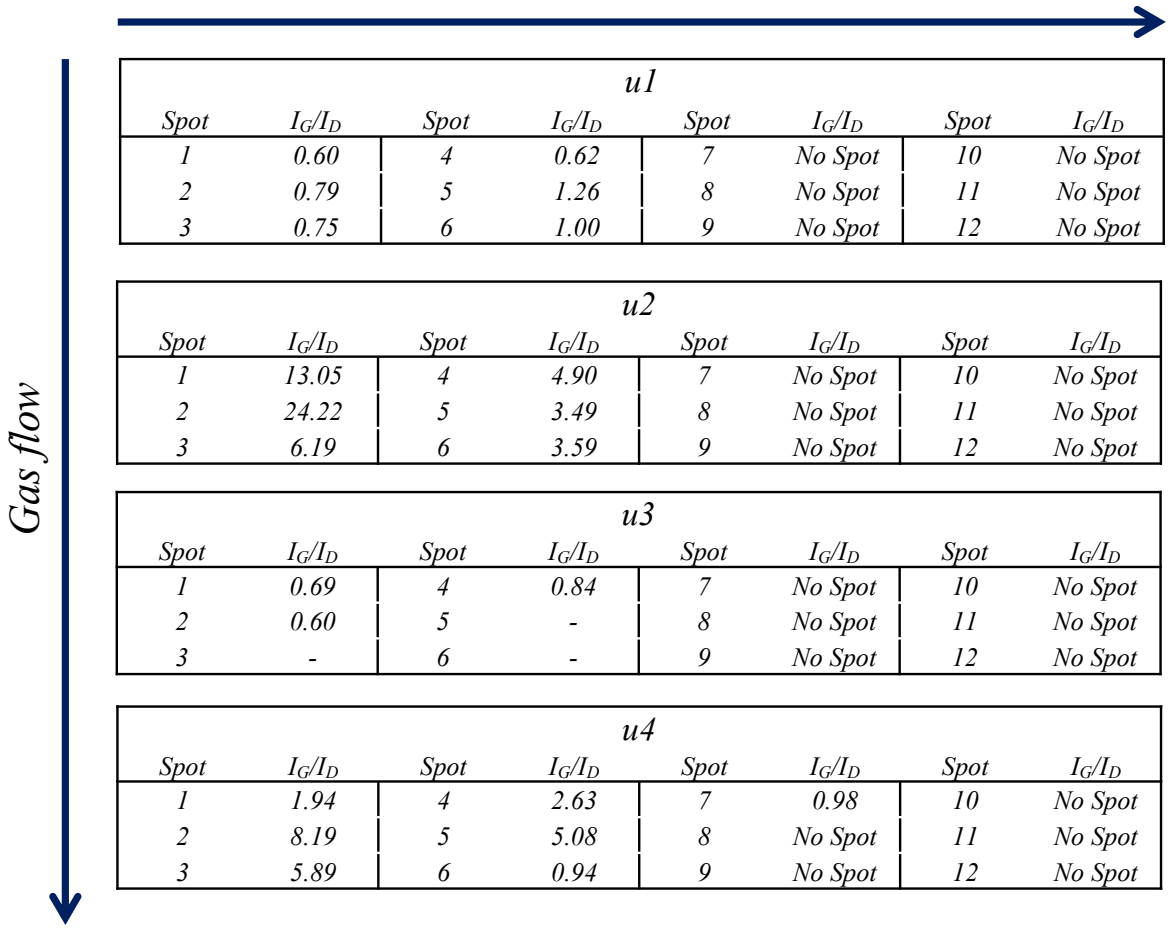

u1

Spot	I_G/I_D	Spot	I_G/I_D	Spot	I_G/I_D	Spot	I_G/I_D
1	0.60	4	0.62	7	No Spot	10	No Spot
2	0.79	5	1.26	8	No Spot	11	No Spot
3	0.75	6	1.00	9	No Spot	12	No Spot

u2

Spot	I_G/I_D	Spot	I_G/I_D	Spot	I_G/I_D	Spot	I_G/I_D
1	13.05	4	4.90	7	No Spot	10	No Spot
2	24.22	5	3.49	8	No Spot	11	No Spot
3	6.19	6	3.59	9	No Spot	12	No Spot

u3

Spot	I_G/I_D	Spot	I_G/I_D	Spot	I_G/I_D	Spot	I_G/I_D
1	0.69	4	0.84	7	No Spot	10	No Spot
2	0.60	5	-	8	No Spot	11	No Spot
3	-	6	-	9	No Spot	12	No Spot

u4

Spot	I_G/I_D	Spot	I_G/I_D	Spot	I_G/I_D	Spot	I_G/I_D
1	1.94	4	2.63	7	0.98	10	No Spot
2	8.19	5	5.08	8	No Spot	11	No Spot
3	5.89	6	0.94	9	No Spot	12	No Spot

Table S5. Raman results obtained with the Rh5 foams after reaction. Effect of longitudinal and radial positions on the I_G/I_D ratios (see Figure S5).

Radius foam →

Gas flow ↓

u1

Spot	I_G/I_D	Spot	I_G/I_D	Spot	I_G/I_D	Spot	I_G/I_D
1	0.88	4	-	7	No Spot	10	No Spot
2	6.84	5	9.30	8	No Spot	11	No Spot
3	1.38	6	8.51	9	No Spot	12	No Spot

u2

Spot	I_G/I_D	Spot	I_G/I_D	Spot	I_G/I_D	Spot	I_G/I_D
1	6.01	4	4.92	7	1.37	10	0.95
2	5.62	5	8.49	8	1.34	11	3.37
3	4.79	6	8.37	9	2.74	12	0.79

u3

Spot	I_G/I_D	Spot	I_G/I_D	Spot	I_G/I_D	Spot	I_G/I_D
1	13.64	4	4.05	7	12.84	10	14.62
2	10.91	5	1.36	8	16.82	11	14.24
3	1.07	6	0.81	9	0.64	12	1.86

u4

Spot	I_G/I_D	Spot	I_G/I_D	Spot	I_G/I_D	Spot	I_G/I_D
1	1.04	4	1.08	7	0.85	10	0.99
2	1.31	5	0.98	8	0.81	11	0.91
3	2.66	6	0.94	9	1.34	12	3.47